Bull. Chem. Soc. Ethiop. **2022**, 36(1), 73-84.
DOI: https://dx.doi.org/10.4314/bcse.v36i1.7

ISSN 1011-3924
Printed in Ethiopia
Online ISSN 1726-801X

SYNTHESIS, SPECTROSCOPIC CHARACTERIZATIONS AND DFT STUDIES ON THE METAL COMPLEXES OF AZATHIOPRINE IMMUNOSUPPRESSIVE DRUG

Amnah Mohammed Alsuhaibani[1], Moamen S. Refat[2*], Abdel Majid A. Adam[2], Mohamed I. Kobeasy[2], Deo Nandan Kumar[3] and Sonam Shakya[4]

[1]Department of Physical Sport Science, College of Education, Princess Nourah bint Abdulrahman University, P.O. Box 84428, Riyadh 11671, Saudi Arabia
[2]Department of Chemistry, College of Science, Taif University, P.O. Box 11099, Taif 21944, Saudi Arabia
[3]Department of Chemistry, Deshbandhu College, Kalkaji, New Delhi – 110019, India
[4]Department of Chemistry, Faculty of Science, Aligarh Muslim University, Aligarh 202002, India

(Received March 4, 2022; Revised March 17, 2022; Accepted March 17, 2022)

ABSTRACT. A complex of the immunosuppressive drug azathioprine with Cr(II), Mn(II), Fe(II), Zn(II), Cu(II), Ni(II), and Co(II) were synthesized and characterized through spectroscopic and thermal studies. The infrared spectra show the coordination of azathioprine via N(9) to the metal, also, the range around 640–650 cm^{-1} remains unchanged in the complexes, indicating the possibility that the ether group may not be involved in the binding. Thermogravimetric analysis (TG), thermogravimetric derivational analysis (DTG), and differential thermogravimetric analysis (DTA) have been studied in the temperature range from 0 °C to 1000 °C. The study of pyrolysis showed that all complexes decompose in more than one step and that the final decomposition product is metal oxide. The DFT (density functional theory) with B3LYP/6-31G++ level of theory was used to study the optimized geometry, HOMO→LUMO energy gap, and molecular electrostatic potential map of azathioprine before and after deprotonation.

KEY WORDS: Azathioprine, Spectral study, Thermal study, Decomposition products, DFT

INTRODUCTION

Medicinal drugs have different functional groups that can bind to metal ions present in the human body [1, 2]. Azathioprine, 6-(1-methyl-4-nitro-5-imidazolithio)-9H-purine is a purine homolog and acts as an immunosuppressive drug used in organ transplantation and autoimmune diseases [3-5]. It is also used to treat Crohn's disease and rheumatoid arthritis [6]. It stops the enzyme amido-phosphoribosyl transferase and prevents the synthesis of RNA and DNA from cells [7]. The stability of complexes with medicinal drugs plays an interesting role in their biological and chemical activities. Azathioprine was prepared as a metabolically active but disguised prodrug from 6-mercaptopurine in the hope that addition of a sulfur atom substitute of 6-mercaptopurine would affect the distribution and metabolism of the drug, thus improving the targeting of the drug towards tumor cells [8]. It works like slow-release prodrug for 6-mercaptopurine due to its proximity to the ortho-nitro group and susceptible to be attacked by nucleophiles and sulfhydryl groups in biological media.

One putative mechanism of action of slow-acting antirheumatic medicines calls for the contribution of their copper compounds to destroy extracellular superoxide radicals like superoxide dismutase mimetics [9]. Glutathione breaks down azathioprine in the liver to produce 6-mercaptopurine and 1-methyl-4-5 (S-glutathionyl) imidazole [10]. As a thiopurine, azathioprine acts as a purine antagonist, interfering with biochemical processes involving endogenously occurring purines, which are essential components of RNA, DNA, and some coenzymes [11, 12].

*Corresponding author. E-mail: moamen@tu.edu.sa

Several mineral compounds have been synthesized from azathioprine with the aim of developing a compound with enhanced chemotherapeutic activity and/or selectivity relative to the parent drug [13, 14]. Determining which chemical agents favor one binding site over another can influence the design and synthesis of slow-release drugs.

Azathioprine contains a few highly versatile binding sites (a thioether bridge, 4 nitrogen atoms of purine ring, and a nitrogen atom plus a nitro group of an imidazole substituent which are likely to be able to coordinate with metals [15]. On neutral azathioprine as an N(9)-H tautomer in the crystal structure of azathioprine [16]. By deprotonation or tautomerization of azathioprine, all four N atoms in the purine ring become potential coordination sites for metal ions [13, 15] cleavage chemically to produce 6-mercaptopurine in red blood cells [17] by the enzyme glutathione-S-transferase [18]. More than 80% of azathioprine is converted to 6-mercaptopurine [19, 20]. It's also transformed to 8-hydroxy-azathioprine by the enzyme aldehyde oxidase, which is then converted to an inactive metabolite, 6-thiouric acid, by xanthine oxidase [21]. Minerals in chelated forms are better transported into the cell [22].

In the current study, metal complexes of azathioprine were prepared and characterized with chromium, manganese, iron, cobalt, nickel, copper, and zinc. The primary goal of the present research is to study the thermal and spectral behavior of the synthesized complexes. DFT studies with B-3LYP/ 6-31G++ level of theory was employed to generate optimized structure for azathioprine (AZA) before and after deprotonation (AZA^-) with minimal energy and to study the preferential binding sites through MEP map.

EXPERIMENTAL

Materials

The chemicals and reagents used in this article were received from "Merck Chemical Company" and started in preparation without other purification.

Instrumentation

Analysis Name	Instrument Name
Elemental analyses	Perkin–Elmer CHN 2400
Magnetic measurements	Sherwood scientific magnetic balance
Infrared spectra	Bruker FTIR Spectrophotometer
^{1}H-NMR spectra	Varian Gemini 200 MHz spectrometer
DTA, TGA and DTG thermal analysis	Schimadzu TGA–50H thermal analyzer
X-band EPR spectra	Varian model E-112 EPR spectrometers

Synthesis

A metal divalent chlorides "MCl_2" solution of (0.1 mol, MCl_2 = $MnCl_2$, $FeCl_2$, $CoCl_2$, $NiCl_2$, $CuCl_2$, $ZnCl_2$, $CrCl_2$) in methanol was treated under stirring with an aqueous solution of (0.1 mol) azathioprine (Figure 1). The reaction mixtures were stirred under reflux at 60 ºC for 3–4 h, the precipitates were filtered off. The resulting solid product was washed twice with acetone and dried in a vacuum. Yield of corresponding azathioprine metal complexes were 70–80%. The metal salts were used directly without any further purification.

Density functional theory

Gaussian 09RevD.01 [23] was used for DFT (density functional theory) studies. Pople's basic set B3LYP/6-31G++ was applied with gradient corrected correlation [24]. The same basic set was used to obtain the optimized structures. Electrostatic potential map (MEP), LUMO (lowest unoccupied molecular orbital), and HOMO (highest occupied molecular orbital) were obtained [25]. The Frontier Molecular orbitals help in determining the chemical stability of the system. For visualization ChemCraft 1.5 software [26] was used.

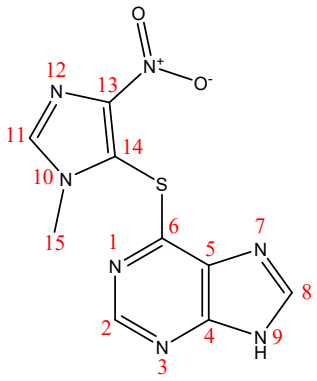

Figure 1. Structure of azathioprine.

RESULTS AND DISCUSSION

All the Cr(II), Mn(II), Fe(II), Co(II), Ni(II), Cu(II), and Zn(II) azathioprine complexes are stable at room temperature, hydrated, insoluble in water and soluble in common organic solvents such as DMF and DMSO. The analytical and physical data of the synthesized complexes are given in Table 1, spectral and thermal stability data (Tables 2 and 3) are compatible with the suggested molecular formula $[C_9H_7N_7O_2SCl_2M].3H_2O$ (M = Cr^{2+}, Mn^{2+}, Fe^{2+}, Co^{2+}, Ni^{2+}, Cu^{2+}, and Zn^{2+}). The molar conductances are in the 10-15 $ohm^{-1}cm^2mol^{-1}$ range, indicating a non-electrolytic nature [2]. Many attempts were made to grow a single crystal but unfortunately, they were failed. Reaction of azathioprine with metal salts ($MnCl_2$, $FeCl_2$, $CoCl_2$, $NiCl_2$, $CuCl_2$, $ZnCl_2$, $CrCl_2$) using (1:1) molar ratios in methanol/H_2O (50:50 v/v) gives complexes (**1-7**). The composition of the complexes formed depends on metal salts, and the molar ratio. The elemental analyses of the complexes listed in the experimental section establish the 1:1 ratio of metal: azathioprine for all the metals used.

Table 1. The molecular weight, color, percentage of carbon, hydrogen, nitrogen, and sulphur elements of Cr(II), Mn(II), Fe(II), Co(II), Ni(II), Cu(II), and Zn(II) azathioprine complexes.

Complexes	M.Wt	Color	[Calculated/(Found)]			
			% C	% H	% N	% S
1. $[C_9H_7N_7O_2SCl_2Cr].3H_2O$	454.26	Green	23.77(23.75)	2.86(2.85)	21.57(21.56)	7.05(7.00)
2. $[C_9H_7N_7O_2SCl_2Mn].3H_2O$	457.21	Brown	23.62(23.61)	2.84(2.84)	21.43(21.42)	7.01(7.00)
3. $[C_9H_7N_7O_2SCl_2Fe].3H_2O$	458.12	Brown	23.57(23.56)	2.84(2.84)	21.39(21.36)	7.00(7.00)
4. $[C_9H_7N_7O_2SCl_2Co].3H_2O$	461.20	Dark green	23.42(23.40)	2.82(2.82)	21.25(21.25)	6.95(6.90)
5. $[C_9H_7N_7O_2SCl_2Ni].3H_2O$	460.96	Light green	23.43(23.42)	2.82(2.82)	21.26(21.26)	6.95(6.92)
6. $[C_9H_7N_7O_2SCl_2Cu].3H_2O$	465.82	Green	23.18(23.18)	2.79(2.78)	21.03(21.00)	6.88(6.87)
7. $[C_9H_7N_7O_2SCl_2Zn].3H_2O$	467.65	Yellow	23.09(23.00)	2.78(2.78)	20.95(20.95)	6.85(6.80)

IR spectra

The IR spectrum of azathioprine–chromium complex given in Figure 2 (representative spectrum) and tentative band assignments of all complexes are given in Table 2. In the IR spectra of all complexes, no significant peaks were observed in 2500-4000 cm^{-1}. This indicates deprotonation of N(9) nitrogen upon coordination with metal [27]. After complex formation, a change in band frequencies in the range 1570-1590 cm^{-1} is observed due to redistribution of electron density of the ring [28, 29]. The splitting of band of free ligand at 1234 cm^{-1} on complexation is due to the coordination of N(9) nitrogen with metal [27]. The band around 640-650 cm^{-1} remains unshifted in complexes, indicates possibility of non-participation of thioether group from binding [30, 31].

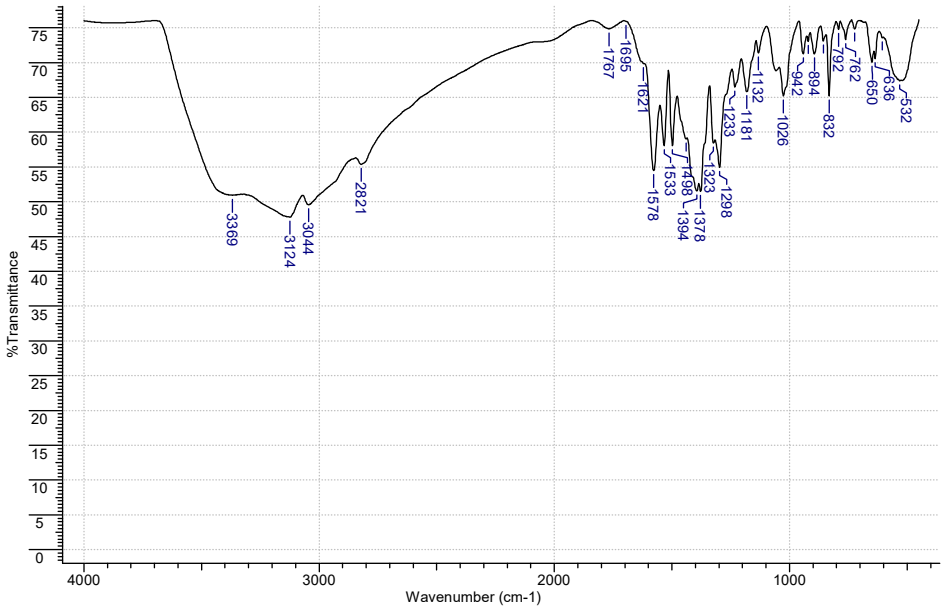

Figure 2. IR spectrum of chromium(II)-azathioprine complex.

ESR spectra

The ESR spectrum of Cu(II)-azathioprine complex was scanned at room temperature. Copper-azathioprine complexes displayed an "isotropic" sharp signal (g = 2.097) which is due to less "dipolar interaction" and "spin-lattice relaxation" [32-35] of the "coordinated ligand" and "spin exchange interaction" between Cu(II) ions [36]. The hyperfine coupling cannot be resolved due to the metal ion (A^{Cu}). Planar, sp^2-type conformation, nitrogen shows a large superfine coupling constant (shf) than tetrahedral nitrogen, sp^3 (lower s). The distortion effect from the planar matrix to the tetrahedral matrix in the first coordination domain may also lead to some decrease in the nitrogen shf coupling [37], since it leads to reduced interference between the non-paired copper electron orbital with the orbital and the ligand orbital and thus causes a lower density Rotation on nitrogen and consequently, the nitrogen coupling constants decrease.

^{1}H NMR spectra

At room temperature, the ^{1}H–NMR spectrum of azathioprine [38] in DMSO–d_6 shows three peaks at 8.58, 8.55 and 8.25 ppm are assigned to H(2), H(8), and H(11) aromatic protons, respectively. The N(9)-H resonates at 13.88 ppm. The H(11) proton of the 1-methyl-4-nitroimidazole ring is resonated at the upfield of the purine protons. The pyrimidine ring is a π-electron deficient system, while the imidazole ring is a π-electron rich system [39]. The zinc-azathioprine complex shows downfield shift for H(2) and H(8) only while H(11) is observed to be unshifted in comparison to azathioprine [40]. The downfield shifts of the azathioprine protons upon zinc(II) coordination with ring nitrogens of purines, results in shift of electron density, which makes the proton more acidic adjacent to the binding site [40-42]. At the same time, due to deprotonation of azathioprine anion (AZA^-), localization of electron density at the same binding position makes H(8) shielded [43, 44].

Table 2. IR spectral band assignments of azathioprine and its metal complexes.

Compound	$\nu_{N(9)-H}$	ν_{C-H} (aromatic)	$\nu_{N(9)-H}$ $\nu_{C=C}$ $\nu_{C=N}$	$\nu_{C=C}$ $\nu_{C=N}$	$\nu_{C(4)-N(9)}$ $\delta_{C(8)-H\ N(9)}$	$\nu_{C(8)-N(9)}$ $\nu_{C(8)-N(7)}$ $\delta_{N(9)-H}$	$\delta_{N(9)-H}$ $\delta_{N(7)-C(8)}$ $\delta_{N(9)-C(8)}$	ν_{C-S-C} γ ring	$\nu_{sym}(NO_2)$ $\nu_{asym}(NO_2)$
Azathioprine	3192w 3121b 2976b 2807b	3108s 3020w	1595sh	1579s	1498s	1374s 1350s 1303s	1234s	636m	1531s 1350w
Cr(II)	-	3124w 3044w	1578m	1498m	1394s	1378s 1323w 1298s	1233w	650w	1533m
Mn(II)	-	3123b	1579w	1498w	1392s	1376s 1359w 1300m	1233m	648b	1531m
Fe(II)	-	3122s 3110sh 3046w	1579s	1498s	1392s 1402s	1374s 1350w 1325m	1234s	636s 648sh	1531m
Co(II)	-	3122b	1578m	1499m	1378s	1299m	1223w	633sh 650w	1535m
Ni(II)	-	3100b	1578m	1500m	1379s	1300s	1222m	635sh 650w	1536m
Cu(II)	-	3111w 2953w 2924m	1579m	1498w	1376m	1298m	1228w	631sh 649w	1531w
Zn(II)	-	3124s 3080sh 3030w	1553s 1554s	1499m	1400s 1379s	1330s	1224s	628sh 651s	1534m

b = broad; w = weak; s = strong; sh =shoulder; m = medium.

Thermal studies

To establish a different decomposition process and to confirm the proposed chemical measurement, the thermal behavior of the complexes was investigated. Table 3 summarizes the findings of the thermal analysis. A very good relationship between the calculated and obtained weight loss values were observed. The different species lost in different stages of decomposition are given in Table 3. TG, DTA, and DTG data are in well agreement. All complexes decompose in more than one step giving metal oxide as a final residual product. The TG, DTG, and DTA curves of azathioprine–chromium complex given in figure 3 (representative figure) and tentative band assignments of all complexes are given in Table 3.

From TG, the decomposition of $[C_9H_7N_7O_2SCl_2Cr].3H_2O$ takes place within the 30–900 ºC temperature range to give CrO as a residual solid product. The 1st, 2nd, 3rd, 4th and 5th decomposition steps of $[C_9H_7N_7O_2SCl_2Cr].3H_2O$ complex presence between 30–180 ºC, 185–262 ºC, 264–430 ºC, 432–580 ºC, and 585–900 ºC, respectively, which correlates the loss of $2H_2O$, $H_2O + Cl_2$, $(NO_2 + 3/2\ N_2 + CH_4 + 5C + S)$, 2 CN, $½\ H_2 +$ CN, respectively. The weight loss percentages observed were 9.03%, 20.64%, 43.68%, 12.92%, 7.52% as against the calculated values of 7.92%, 19.59%, 43.15%, 11.45% and 5.94% for the I, II, III, IV and V steps, respectively. The five decomposition stages of $[C_9H_7N_7O_2SCl_2Cr].3H_2O$ complex located at 250 ºC, 425.95 ºC, and 490 ºC as a DTA exothermic peaks, respectively, whereas DTG gives peaks are present at 75 ºC, 180 ºC, 240.38 ºC, 424.62 ºC, 490 ºC, 890 ºC, respectively.

From TG, the thermal decomposition of $[C_9H_7N_7O_2SCl_2Mn].3H_2O$ complex occurs within 30–562 ºC temperature range to give MnO as a solid residual. The 1st, 2nd, and 3rd decomposition stages of $[C_9H_7N_7O_2SCl_2Mn].3H_2O$ complex take place between 30–88 ºC, 89–340 ºC, and 341–562 ºC, respectively, which correlates the of $3\ H_2O$, $HCN + Cl_2$, $(NO_2 + CH_4 + CN + 4C + S)$,

respectively. The weight loss percentages observed were 10.95%, 21.12%, and 36.45%, as against the calculated values of 11.81%, 21.43%, and 36.74% for the three steps, respectively. The DTA exothermic peaks present at 226.47 ºC, and 476.29 ºC whereas the DTG peaks occur at 40.40 ºC, 231.72 ºC, and 478.43 ºC.

From TG, the decomposition of $[C_9H_7N_7O_2SCl_2Fe].3H_2O$ presence within the 30–517 ºC temperature range to produced FeO as a final residue. The first-to-fourth decomposition stages of $[C_9H_7N_7O_2SCl_2Fe].3H_2O$ complex take place within 30–154 ºC, 155–210 ºC, 213–390 ºC, and 391–517 ºC, respectively, which correlates the loss of 1.5 H_2O, $H_2O + Cl_2$, (NO_2 + 3/2 N_2 + CH_4 +5C), (3 CN + S), respectively. The weight loss percentages observed were 5.85%, 18.42%, 37.49%, 25.39% as against the calculated values of 5.89%, 19.42%, 35.80%, 24.01% for the four decomposition steps, respectively. The DTA exothermic peaks located at 213.74 ºC, and 497.33 ºC, respectively, whereas the DTG peaks are existed at 80 ºC, 202 ºC, 290 ºC, 430 ºC, and 498.93 ºC, respectively for all four stages of decomposition of $[C_9H_7N_7O_2SCl_2Fe].3H_2O$.

From TG, the decomposition of $[C_9H_7N_7O_2SCl_2Co].3H_2O$ complex is present at the temperature range of 30–604 ºC to yield a solid residual product of CoO. The 1st – 3rd decomposition stages of the $[C_9H_7N_7O_2SCl_2Co].3H_2O$ complex occur between 30–182 ºC, 183–514 ºC, and 515–604 ºC, respectively, which correlates the of 2.5H_2O, (0.5 H_2O + Cl_2+ NO_2 + N_2 + CH_4 + C) and (2.5 CN + S + 4C), respectively. The weight loss percentages observed were 9.73%, 39.94%, and 31.75% as against the calculated values of 9.76%, 39.46%, and 31.44% for the three steps, respectively. The DTA exothermic peaks are existed at 279.00 ºC, 546.33 ºC, and 595.00 ºC, whereas the DTG peaks are located at 70.61 ºC, 204.04 ºC, 432.38 ºC, and 551.34 ºC, respectively for the decomposition of $[C_9H_7N_7O_2SCl_2Co].3H_2O$ for all the three stages.

From TG, the decomposition of $[C_9H_7N_7O_2SCl_2Ni].3H_2O$ complex take place within the 30–616 ºC temperature range to produce a solid NiO residue. The first-to-fourth decomposition stages of $[C_9H_7N_7O_2SCl_2Ni].3H_2O$ complex presence at 30–196 ºC, 197–254 ºC, 255–492 ºC, and 493–616 ºC, respectively, which correlates the of 3 H_2O, 0.5 Cl_2 + CH_4, (0.5 Cl_2 + NO_2 +N_2 + C), (3 CN + S + 4C), respectively. The weight loss percentages observed were 10.62%, 12.58%, 25.27%, 34.73% as against the calculated values of 11.71%, 11.17%, 26.36%, 34.28% for the four steps, respectively. The DTA exothermic peaks are located at 300.70 ºC, 507.70 ºC and 563.43 ºC, respectively, whereas the DTG peaks are existed at 83.36 ºC, 244.86 ºC, and 564.48 ºC, respectively for the fourth decomposition stages of $[C_9H_7N_7O_2SCl_2Ni].3H_2O$.

From TG curve, the thermal decomposition stages of $[C_9H_7N_7O_2SCl_2Cu].3H_2O$ complex take place within the temperature range of 30–573 ºC to give solid residue from CuO. The first-to-third decomposition stages of $[C_9H_7N_7O_2SCl_2Cu].3H_2O$ complex presence between 30–194 ºC, 195–456 ºC, and 457–573 ºC, respectively, which correlates the loss of 2 H_2O, (H_2O + Cl_2 + N_2+ C) and (3 CN + S + 5C + CH_4 + NO_2), respectively. The weight loss percentages observed were 7.67%, 27.63%, and 48.22% as against the calculated values of 7.73%, 27.69%, and 49.80% for the three steps, respectively. The DTA exothermic peaks are present at 214 ºC, 500 ºC, and 558.70 ºC, whereas DTG curve gives 212.81 ºC, and 555.33 ºC peaks, respectively, for all three decomposition stages of $[C_9H_7N_7O_2SCl_2Cu].3H_2O$ complex.

From the TG curve, the thermal decomposition of $[C_9H_7N_7O_2SCl_2Zn].3H_2O$ complex located within the temperature range of 30–648 ºC to yield a zinc oxide, ZnO as solid residue. The four thermal decomposition stages of $[C_9H_7N_7O_2SCl_2Zn].3H_2O$ complex presence at 30–163 ºC, 164–232 ºC, 233–478 ºC, and 479–648 ºC ranges, respectively, which correlates the loss of H_2O, 2H_2O, Cl_2 + CH_4 + 0.5 NO_2 and remaining moiety respectively. The weight loss percentages observed were 3.09%, 8.54%, 22.46%, 62.08% as against the calculated values of 3.85%, 7.70%, 23.55% for the four steps, respectively. The DTA exothermic peaks are located at 200 ºC, 550 ºC, and 625.32 ºC, respectively, whereas the DTG gives peaks are present at 80 ºC, 223.74 ºC, 300 ºC, 350 ºC, 600 ºC, and 622 ºC, respectively, for the decomposition of $[C_9H_7N_7O_2SCl_2Zn].3H_2O$ of all the four stages. The literature contains different interpretations of the relative order of thermal stability of the complexes [45, 46]. The order of decomposition reaction in each case is unity.

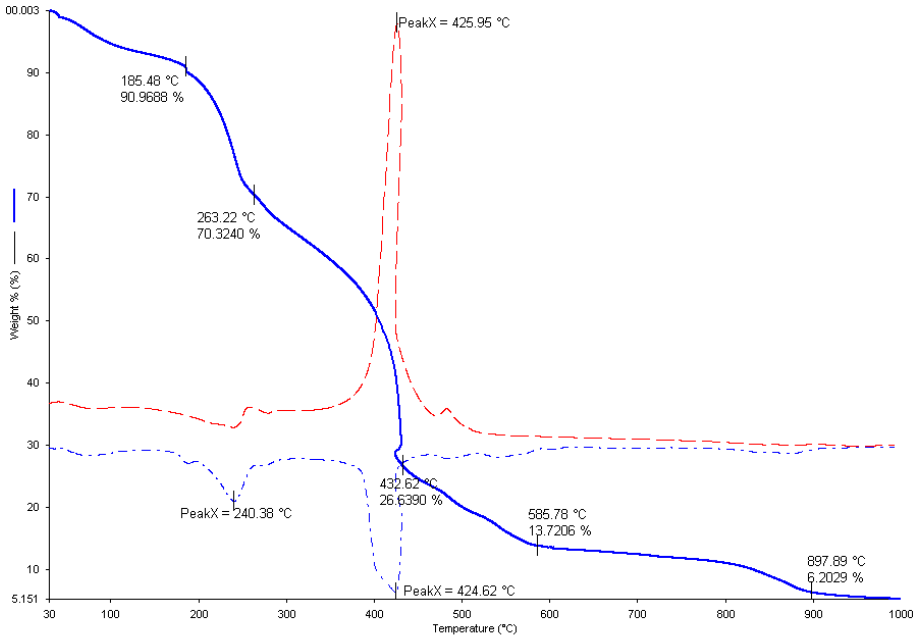

Figure 3. TG (blue –), DTA (red --) and DTG (blue …) curves of Cr(II) complex.

Magnetic measurements

Gouy's method was utilized for magnetic susceptibility measurements using the following equation 1 [47]:

$$Xg = C\,(R - R_0)/10^{-9}\,M \quad (1)$$

where "Xg= mass susceptibility per gram of sample", "C is the calibration constant of the instrument", "R is the balance reading for the sample and tube", "R_0 is the balance reading for the empty tube", "M is the weight of the sample in grams" and "T is the absolute temperature". Magnetic measurements were performed on a Sherwood scientific magnetic balance according to the Gouy's method [47]. The Cr(II), Mn(II), Fe(II), Co(II) complex showed a magnetic moment of 3.85 B.M., 5.90 B.M., 4.89 B.M., 3.82 B.M. respectively with agreement with hybridization of sp^3d^2, on the other hand, the Ni(II) and Cu(II)have 2.65 B.M. and 1.71 B.M., respectively. This may be due to Jahn Teller distortion, which results in distortion in structure from octahedral geometry [48].

DFT studies

The optimized structures of azathioprine were obtained through B3LYP/6-31G++ level of theory. Azathioprine has -1278.611130 a.u. minimum SCF energy after 23 steps of optimization, while after deprotonation it was found to be -1277.895903 a.u. after 23 optimization steps. The optimized structure with strain-free lattice constants of azathioprine (AZA and AZA^-) is shown in Figure 4. The electrostatic potentials strength of azathioprine before and after deprotonation is represented by MEP map (molecular electrostatic potential map) (Figure 5). Electropositive region is displayed with blue color and electronegative with red. The most electropositive region is around O2 and O3 atoms, while the most electronegative region is around N8 atom of azathioprine (Figure 5a). These results signify the higher tendency of deprotonation of N8 atom

and be available as a preferential binding site for the electrophilic and nucleophilic attacks [49]. Figure 5b shows the creation of electronegative region around N8 atom due to deprotonation. The MEP surface maps are plotted from deep red as -7.928 e^{-2} to deep blue as +7.928 e^{-2} and -7.928 e^{-2} to +7.928 e^{-2} in the color scale for azathioprine before and after protonation of N8 atom, respectively [50].

Table 3. Thermal analysis data of azathioprine complexes.

Complex	Decomposition step	Temperature range (°C)	Weight loss found/(calculated)	Assignments
1. $[C_9H_7N_7O_2SCl_2Cr].3H_2O$	I	30 - 180	9.03 (7.92)	- $2H_2O$
	II	185 - 262	20.64(19.59)	- H_2O+Cl_2
	III	264 - 430	43.68(43.15)	- $NO_2+3/2N_2+CH_4+5C+S$
	IV	432 - 580	12.92(11.45)	- 2CN
	V	585 - 900	7.52(5.94)	- $1/2H_2+CN$
2. $[C_9H_7N_7O_2SCl_2Mn].3H_2O$	I	30 - 88	10.95(11.81)	- $3H_2O$
	II	89 - 340	21.12(21.43)	- Cl_2+HCN
	III	341 - 562	36.45(36.74)	- $NO_2+CN+CH_4+4C+S$
3. $[C_9H_7N_7O_2SCl_2Fe].3H_2O$	I	30 - 154	5.85(5.89)	- $1.5H_2O$
	II	155 - 210	18.42(19.42)	- H_2O+Cl_2
	III	213- 390	37.49(35.80)	- $NO_2+3/2N_2+CH_4+5C$
	IV	391 - 517	25.39(24.01)	- 3CN+S
4. $[C_9H_7N_7O_2SCl_2Co].3H_2O$	I	30 - 182	9.73(9.76)	- $2.5H_2O$
	II	183- 514	39.94(39.46)	- $0.5H_2O+Cl_2+NO_2+N_2+CH_4+C$)
	III	515 - 604	31.75(31.44)	- 2.5CN+S+4C
5. $[C_9H_7N_7O_2SCl_2Ni].3H_2O$	I	30 - 196	10.62(11.71)	- $3H_2O$
	II	197 - 254	12.58(11.17)	- $CH_4+0.5Cl_2$
	III	255 - 492	25.27(26.36)	- $0.5Cl_2+NO_2+N_2+C$
	IV	493 - 616	34.73(34.28)	- 3CN+S+4C
6. $[C_9H_7N_7O_2SCl_2Cu].3H_2O$	I	30 - 194	7.67(7.73)	- $2H_2O$
	II	195 - 456	27.63(27.69)	- $H_2O+Cl_2+N_2+C$
	III	457 - 573	48.22(49.80)	- $3CN+S+5C+CH_4+NO_2$
7. $[C_9H_7N_7O_2SCl_2Zn].3H_2O$	I	30 - 163	3.09(3.85)	- H_2O
	II	164 - 232	8.54(7.70)	- $2H_2O$
	III	233 - 478	22.46(23.55)	- $Cl_2+CH_4+0.5NO_2$
	IV	479 - 648	62.08(62.05)	-Remaining moiety

Frontier molecular orbitals (FMOs) were obtained through DFT calculations. Electron donors are highest occupied molecular orbitals (HOMO), while electron acceptors are lowest unoccupied molecular orbitals (LUMO). According to the literature the compounds having smaller energy gap are soft in nature, possess low kinetic stability, and higher chemical reactivity [50]. Figure 6 represents the energies associated with LUMO and HOMO with HOMO-LUMO gap. As it can be seen in Table 4, The HOMO–LUMO gap (ΔE) for azathioprine is 4.3373 eV and for azathioprine after deprotonation of N8 atom, ΔE = 4.3541 eV [50], total dipole moment of the molecules (μ) and polarizability (α) were also obtained.

Table 4. The theoretically calculated some molecular properties of AZA and AZA^-.

	E_{HOMO} (Ev)	E_{LUMO} (Ev)	Gap (Ev)	μ (Debye)	A (a.u.)
AZA	-6.7433	-2.4060	4.3373	8.460245	160.595759
AZA^-	-7.2347	-2.8806	4.3541	8.460249	160.595758

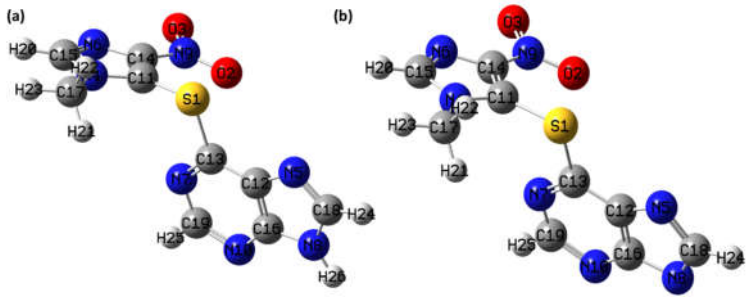

Figure 4. Optimized structure with Mulliken atom numbering of (a) Azathioprine and (b) azathioprine after deprotonation of N8 atom.

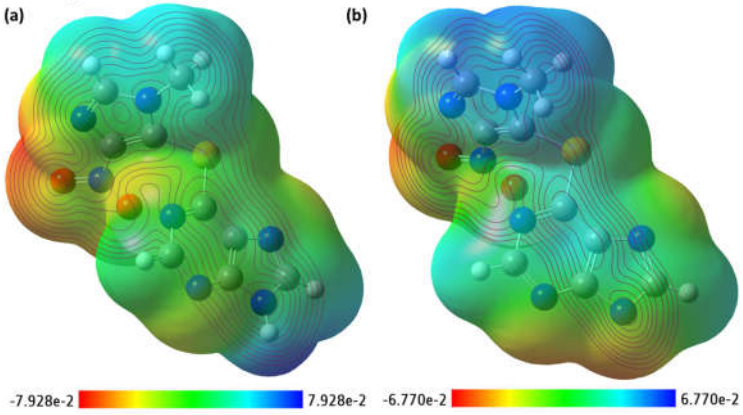

Figure 5. MEP surface map with respective color scales representing electropositive region with blue color and electronegative with red color for (a) azathioprine and (b) azathioprine after deprotonation of N8 atom.

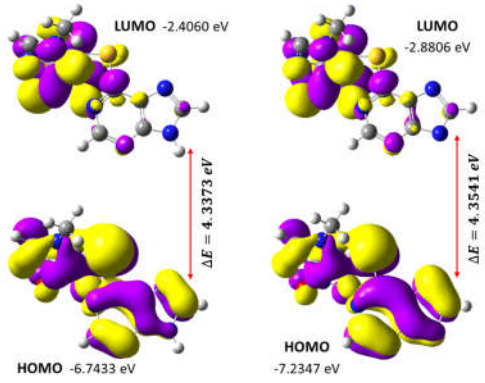

Figure 6. Spatial plot of HOMO and LUMO with their energy gap for Azathioprine (left) and azathioprine after deprotonation of N8 atom (right).

ACKNOWLEDGEMENT

Taif University Researches Supporting Project number (TURSP-2020/01), Taif University, Taif, Saudi Arabia.

REFERENCES

1. Thomas, G. *Fundamentals of Medicinal Chemistry*, John Wiley and Son: London; **2003**.
2. Mendham, J. *Vogel's Textbook of Quantitative Chemical Analysis*, Pearson Education: India; **2006**.
3. Kinlen, L.J. Incidence of cancer in rheumatoid arthritis and other disorders after immunosuppressive treatment. *Am. J. Med*. **1985**, 78, 44-49.
4. Fries, J.F.; Bloch, D.; Spitz, P.; Mitchell, D.M. Cancer in rheumatoid arthritis: A prospective long term study of mortality. *Am. J. Med*. **1985**, 78, 56-59.
5. (a) Kotton, C.N.; Hibberd, P.L. Travel medicine and the solid organ transplant recipient. *Am. J. Transplant*. **2009**, 9, 273-281; (b) Cassetta, I.; Iuliano, G; Filippini, G. Azathioprine for multiple sclerosis. *J. Neurol. Neurosurg. Psychiatry* **2019**, 80, 131-132.
6. Patel, A.A.; Swerlick, R.A.; McCall, C.O. Azathioprine in dermatology: The past, the present and the future. *J. Am. Acad. Dermatol*., **2006**, 55, 369-389.
7. Naveed, S. *Autoimmune Bullous Diseases: Approach and Management*, Springer International Publishing: Switzerland; **2016**; pp. 83.
8. Smaranda, I.; Nila, A.; Manta, C.M.; Samohvalov, D.; Gherca, D.; Baibarac, M. The influence of UV light on the azathioprine photodegradation: New evidences by photoluminescence. *Results Phys*. **2019**, 14, 102443. doi.org/10.1016/j.rinp.2019.102443.
9. Roberts, N.A.; Robinson, P.A. Copper chelates of antirheumatic and anti-inflammatory agents: Their superoxide dismutase-like activity and stability. *Br. J. Rheumatol*. **1985**, 24, 128-136.
10. Elion, G.B. The purine path to chemotherapy. *Biosci Rep*. **1989**, 9, 509-529.
11. Greenberg, G.R.; Jaenicke, L. in *The Chemistry and Biology of Purines* (Wolstenholme, G.E.W.; O'Connor, C.M.; Ed.) Churchill: London; **1957**; pp. 204-232.
12. Periguard, C.; Gosselin, G.; Imbach, J.L. Nucleoside Analogues as Chemotherapeutic Agents: A review. *Nucleosides Nucleotides* **1992**, 11, 903-945.
13. Singh, S.; Gulati, M.; Gupta, R.L. Complexation behaviour of azathioprine with metal ions. *Int. J. Pharm*. **1991**, 68, 105-110.
14. Chifotides, H.T.; Katsaros, N.; Pneumatikakis, G.J. Complexes of azathioprine, a biologically active mercaptopurine derivative, with Pt(II), Pd(II), Rh(III), Ru(III) and Ag(I). *Inorg. Biochem*. **1994**, 56, 249-263.
15. Chifotides, H.T.; Dunbar, K.R.; Matonis, J.H. Unusual structural features of tetrakis (μ-carboxylato)dirhodium(II), an antitumor agent, bound to azathioprine, a biologically active mercaptopurine derivative. *Inorg. Chem*. **1992**, 31, 4628-4634.
16. Acharya, K.R. Crystal structure of 6-[(1-methyl-4-nitroimidazol-5-yl)thio] purine. *Proc. Indian Acad. Sci*., *(Chem. Sci.)* **1984**, 93, 183-187.
17. Sachin, V.; Bendre, A.B.; Joseeph, G.; Shaddock, B.; Ralph, E.; Patton, C.; Vasily, N.; Dobrovolsky, B.; Richard, J.; Albertini, D.; Robert, H.; Heflicch A.B. Lymphocyte Hprt mutant frequency and sperm toxicity in C57BL/6 mice treated chronically with azathioprine. *Mutat. Res*. **2005**, 578, 1-14.
18. Van Scoik, K.G.; Johnson, C.A.; Porter, W.R. The pharmacology and metabolism of the thiopurine drugs 6-mercaptopurine and azathioprine. *Drug Metab. Rev*. **1985**, 16, 157-174.
19. Sandborn, W.J. Azathioprine: state of the art in inflammatory bowel disease. *Scand. J. Gastroenterol. Suppl*. **1998**, 225, 92-99.

20. Cuffari, C.; Hunt, S.; Bayless, T.M. Enhanced bioavailability of azathioprine compared to 6-mercaptopurine therapy in inflammatory bowel disease correlation with treatment efficacy. *Aliment Pharmacol. Ther*. **2000**, 14, 1009-1014.
21. Zimm, S.; Collins, J.M.; Riccardi, R.; O'Neill, D.; Narang, P.K.; Chabner, B.; Poplack, D.G. Variable bioavailability of oral mercaptopurine is maintenance chemotherapy in acute lymphoblastic leukemia being optimally delivered. *New Engl. J. Med*. **1983**, 308, 1005-1009.
22. Cleare, M.L.; Hydes, P.C. in *Metal Ions in Biological Systems*, Sigel, H.; (Ed.), Vol. 11, Dekker: New York; **1980**; p. 1.
23. Frisch, M.J.; Trucks, G.W.; Schlegel, H.B.; Scuseria, G.E.; Robb, M.A.; Cheeseman, J.R.; Montgomery Jr., J.A.; Vreven, T.; Kudin, K.N.; Burant, J.C.; Millam, J.M.; Iyengar, S.S.; Tomasi, J.; Barone, V.; Mennucci, B.; Cossi, M.; Scalmani, G.; Rega, N.; Petersson, G.A.; Nakatsuji, H.; Hada, M.; Ehara, M.; Toyota, K.; Fukuda, R.; Hasegawa, J.; Ishida, M.; Nakajima, T.; Honda, Y.; Kitao, O.; Nakai, H.; Klene, M.; Li, X.; Knox, J.E.; Hratchian, H.P.; Cross, J.B.; Adamo, C.; Jaramillo, J.; Gomperts, R.; Stratmann, R.E.; Yazyev, O.; Austin, A.J.; Cammi, R.; Pomelli, C.; Ochterski, J.W.; Ayala, P.Y.; Morokuma, K.; Voth, A.; Salvador, P.; Dannenberg, J.J.; Zakrzewski, V.G.; Dapprich, S.; Daniels, A.D.; Strain, M.C.; Farkas, O.; Malick, D.K.; Rabuck, A.D.; Raghavachari, K.; Foresman, J.B.; Ortiz, J.V.; Cui, Q.; Baboul, A.G.; Clifford, S.; Cioslowski, J.; Stefanov, B.B.; Liu, G.; Liashenko, A.; Piskorz, P.; Komaromi, I.; Martin, R.L.; Fox, D.J.; Keith, T.; Al-Laham, M.A.; Peng, C.Y.; Nanayakkara, A.; Challacombe, M.; Gill, P.M.W.; Johnson, B.; Chen, W.; Wong, M.W.; Gonzalez, C.; Pople, J.A. Gaussian Inc.: Wallingford, CT; **2004**.
24. Becke, A.D. Density-functional thermochemistry. III. The role of exact exchange. *J. Chem. Phys*. **1993**, 98, 5648-5652.
25. Hariharan, P.C.; Pople, J.A. The effect of d-functions on molecular orbital energies for hydrocarbons. *Chem. Phys. Lett*. **1972**, 16, 217-219.
26. (a) Zhurko, G.A.; Zhurko, D.A. Chemcraft - graphical program for visualization of quantum chemistry computations. Ivanovo, Russia, Academic version 1.5 (2004) **2004**; (b) Akram, M.; Lal, H.; Shakya, S.; Kabir-ud-Din. Multispectroscopic and computational analysis insight into the interaction of cationic diester-bonded gemini surfactants with serine protease α-chymotrypsin. *ACS Omega* **2020**, 5, 3624-3637.
27. Cervantes, G.; Fiol, J.J.; Terron, A.; Moreno, V.; Alabart, J.R.; Aguil, M.; Gomez, M.; Solans, X. Synthesis and characterization of nickel(II) complexes of purine and pyrimidine bases. Crystal and molecular structure of trans-bis(cytosine-O2)bis(ethylenediamine)nickel(II) bis(tetraphenylborate). An unusual metal binding mode of cytosine. *Inorg. Chem*. **1990**, 29, 5168-5173.
28. Cozak, D.; Mardhy, A.; Olivier, M.J.; Beauchamp, A. N7/06 chelation in a complex with an analog of guanine. Preparation, spectroscopic study, and crystal structure of bis(*E*-5-cyclopentadienyl)(theophyllinato)titanium(III). *Inorg. Chem*. **1986**, 25, 2600-2606.
29. Tajmir-Riahi, H.A.; Theophanides, T. Magnesium–nucleotide interaction. Synthesis, structure, ^{1}H, ^{13}C nuclear magnetic resonance and Fourier transform infrared studies of Mg-inosine-5′-monophosphate complexes. *Can. J. Chem*. **1985**, 63, 2065-2072.
30. Socrates, G. *Infrared Characteristic Group Frequencies*, Wiley: New York; **1980**; p. 111.
31. Sheppard, N. The vibrational spectra of some organic sulphur compounds and the characteristic frequencies of C—S linkages. *Trans. Faraday Soc*. **1950**, 46, 429-439.
32. Figgis, B.N. *Introduction to Ligand Fields*, Wiley Eastern Ltd.: London; **1996**; p. 319.
33. Prosser, K.E.; Walsby, C.J. Electron paramagnetic resonance as a tool for studying the mechanisms of paramagnetic anticancer metallodrugs. *Eur. J. Inorg. Chem.* **2017**, 12, 1573-1585.
34. Bindu, P.; Kurup, M.R.P. ESR and electrochemical studies of four-and five-coordinate copper(II) complexes containing mixed ligands. *Trans. Met. Chem.* **1997**, 22, 578-582.

35. Amundsen, A.R.; Whelan, J.; Bosrich, B. Biological analogs. Nature of the binding sites of copper-containing proteins. *J. Am. Chem. Soc.* **1977**, 99, 6730-6739.
36. Bhadbhade, M.M.; Srinivas, D. Effects on molecular association, chelate conformation, and reactivity toward substitution in copper Cu(5-X-salen) complexes, salen2- = N,N'-ethylenebis(salicylidenaminato), X = H, CH3O, and Cl: synthesis, X-ray structures, and EPR investigations. *Inorg. Chem.* **1993**, 32, 5458-5466.
37. Klement, R.; Stock, F.; Elias, H.; Paulus, H.; Pelikan, P.; Valko, M.; Mazur, M. Copper(II) complexes with derivatives of salen and tetrahydrosalen: a spectroscopic, electrochemical and structural study. *Polyhedron* **1999**, 18, 3617-3628.
38. Chifotides, H.T.; Katsaros, N.; Pneumatikakis, G. Complexes of azathioprine, a biologically active mercaptopurine derivative, with Pt(II), Pd(II), Rh(III), Ru(III) and Ag(I). *J. Inorg. Biochem*. **1994**, 56, 249-264.
39. Breitmaier, E.; Voelter, W. *Carbon-C23 NIUR Spectroscopy*, VCH Publishers: New York; **1990**; pp. 80, 281.
40. Hadjiliadis, N.; Theophanides, T. Platinum purine nucleosides I. Interaction of K_2PtX_4 (X = Cl, Br) with adenosine, triacetyladenosine, adenosine-1-oxide and 9-methyladenine. *Inorg. Chim. Acta* **1975**, 16, 67-75.
41. Pneumatikakis, G.; Hadjiliadis, N. Interactions of tetrakis-μ-acetato-dirhodium(II) with adenine nucleosides and nucleotides. *J. Chem. Soc. Dalton Trans*. **1979**, 596-599.
42. Eichhorn, G.L.; Clark, P.; Becker, E.D. Interactions of metal ions with polynucleotides and related compounds. VII. The binding of copper(II) to nucleosides, nucleotides, and deoxyribonucleic acids. *Biochemistry* **1966**, 5, 245-253.
43. Norris, A.R.; Buncel, E.; Taylor, S.E. Metal ion-biomolecule interactions. III. Versatility of metal ion binding to imidazoles. Synthesis and ^{1}H NMR spectroscopic properties of N- and C-bound mercury(II) complexes. *J. Inorg. Biochem.* **1982**, 16, 279-295.
44. Louloudi, M.; Hadjiliadis, N.; Butler, I.S. Solution versus solid state conformation of Group 12 metal complexes of active aldehyde derivatives of thiamine. *J. Chem. Soc. Dalton Trans*. **1992**, 1401-1405.
45. Kumar, D.N.; Garg, B.S. Synthesis and spectroscopic studies of complexes of zinc(II) with N2O2 donor groups. *Spectrochim. Acta A* **2006**, 64, 141-147.
46. Bartyzel, A. Synthesis, thermal study and some properties of N2O4—Donor Schiff base and its Mn(III), Co(II), Ni(II), Cu(II) and Zn(II) complexes. *J. Therm. Anal. Calorim*. **2016**, 127, 2133-2147.
47. Clarke, E.G.C.; Moffat, A.C.; Pharmaceutical Society of Great Britain; Department of Pharmaceutical Sciences. Clarke's Isolation and Identification of Drugs in Pharmaceuticals, Body Fluids, and Post-Mortem Material, 2nd ed.; **1970**.
48. Moffat, A.C. (Ed.) *Pharmaceutical Press*: King of Prussia, PA, USA; Rittenhouse Book Distributors: London, UK; **1986**.
49. Shakya, S.; Khan, I.M.; Ahmad, M. Charge transfer complex based real-time colorimetric chemosensor for rapid recognition of dinitrobenzene and discriminative detection of Fe^{2+} ions in aqueous media and human hemoglobin. *J. Photochem. Photobiol. A Chem*. **2020**, 392, 112402.
50. Refat, M.S.; Saad, H.A.; Gobouri, A.A.; Alsawat, M.; Adam, A.M.A.; Shakya, S.; Gaber, A.; Alsuhaibani, A.M.; El-Megharbel, S.M. Synthesis and spectroscopic characterizations of nanostructured charge transfer complexes associated between moxifloxacin drug donor and metal chloride acceptors as a catalytic agent in a recycling of wastewater. *J. Mol. Liq*. **2022**, 349, 118121. doi.org/10.1016/j.molliq.2021.118121.